Bioactive Materials 43 (2025) 181–194

Contents lists available at ScienceDirect

Bioactive Materials

journal homepage: www.keaipublishing.com/en/journals/bioactive-materials

Exploring the potential of laser-textured metal alloys: Fine-tuning vascular cells responses through *in vitro* and *ex vivo* analysis

Indong Jun [a,h,**], Haneul Choi [b], Hyeok Kim [c], Byoung Chan Choi [d], Hye Jung Chang [b], Youngjun Kim [a], Sung Woo Cho [e], James R. Edwards [f], Suk-Won Hwang [c,g,i], Yu-Chan Kim [c], Hyung-Seop Han [c,*], Hojeong Jeon [c,g,***]

[a] *Environmental Safety Group, Korea Institute of Science & Technology Europe (KIST-EUROPE), Saarbrücken, 66123, Germany*
[b] *Center for Hydrogen Energy Materials, Korea Institute of Science & Technology (KIST), Seoul, 02792, Republic of Korea*
[c] *Biomaterials Research Center, Biomedical Research Division, Korea Institute of Science and Technology (KIST), Seoul, 02792, Republic of Korea*
[d] *Laser Surface Texturing Group, AYECLUS, Gyeonggi-do, 14255, Republic of Korea*
[e] *Division of Cardiology, Department of Internal Medicine, Inje University Ilsan Paik Hospital, College of Medicine, Inje University, Gyeonggi-do, 10380, Republic of Korea*
[f] *Nuffield Department of Orthopaedics, Rheumatology and Musculoskeletal Sciences (NDORMS), University of Oxford, Oxford, OX3 7LD, United Kingdom*
[g] *KU-KIST Graduate School of Converging Science and Technology, Korea University, Seoul, 02841, Republic of Korea*
[h] *Department of Molecular Science and Technology, Ajou University, Suwon, 16499, Republic of Korea*
[i] *Department of Integrative Energy Engineering, Korea University, Seoul, 02841, Republic of Korea*

A R T I C L E I N F O

Keywords:
Laser texturing
Metal alloy
Surface modification
Vascular cells
Ex vivo angiogenesis assays

A B S T R A C T

Medical stents are vital for treating vascular complications and restoring blood flow in millions of patients. Despite its widespread effectiveness, restenosis, driven by the complex interplay of cellular responses, remains a concern. This study investigated the reactions of vascular cells to nano/microscale wrinkle (nano-W and micro-W) patterns created on laser-textured nitinol (NiTi) surfaces by adjusting laser processing parameters, such as spot overlap ratio and line overlap ratio. Evaluation of topographical effects on endothelial and smooth muscle cells (SMCs) revealed diverse morphologies, proliferation rates, and gene expressions. Notably, microscale wrinkle patterns exhibited reduced monocyte adhesion and inflammation-related gene expression, demonstrating their potential applications in mitigating vascular complications after stent insertion. Additionally, an *ex vivo* metatarsal assay was utilized to bridge the gap between *in vitro* and *in vivo* studies, demonstrating enhanced angiogenesis on laser-textured NiTi surfaces. Laser-textured NiTi exhibits a guided formation process, emphasizing their potential to promote swift endothelialization. These findings underscore the efficacy of laser texturing for tailored cellular interactions on metallic surfaces and offer valuable insights into optimizing biocompatibility and controlling cellular responses, which may pave the way for innovative advances in vascular care and contribute to the ongoing improvement of stent insertion.

Abbreviations: ECs, Endothelial Cells; SMCs, Smooth Muscle Cells; NiTi, Nitinol (Nickel Titanium) Alloy; SEM, Scanning Electron Microscopy; AFM, Atomic Force Microscopy; XRD, X-ray diffraction; EDS, Energy-Dispersive Spectroscopy; HAADF STEM, High-Angle Annular Dark-Field Scanning Transmission Electron Microscopy; EGM, Endothelial Growth Medium; RPMI, Roswell Park Memorial Institute; FITC, Fluorescein Isothiocyanate; DAPI, 4′,6-Diamidino-2-Phenylindole; BrdU, 5-Bromo-2′-Deoxyuridine; LSM, Laser Scanning Microscope; TNF-α, Tumor Necrosis Factor-Alpha; nano-W, Nano-wrinkle; pNW, Patterned nano-wrinkle; micro-W, Micro-wrinkle; pMW, Patterned micro-wrinkle.

Peer review under responsibility of KeAi Communications Co., Ltd.

* Co-corresponding author.
** Co-corresponding author. Environmental Safety Group, Korea Institute of Science & Technology Europe (KIST-EUROPE), Saarbrücken, 66123, Germany.
*** Co-corresponding author. Biomaterials Research Center, Biomedical Research Division, Korea Institute of Science and Technology (KIST), Seoul, 02792, Republic of Korea.
E-mail addresses: indong.jun@kist-europe.de (I. Jun), hyuhan@kist.re.kr (H.-S. Han), jeonhj@kist.re.kr (H. Jeon).

https://doi.org/10.1016/j.bioactmat.2024.09.019
Received 14 March 2024; Received in revised form 4 September 2024; Accepted 15 September 2024

1. Introduction

Millions of patients undergo angioplasty each year, utilizing medical devices like bare metal or drug-eluting stents; this procedure has become the cornerstone for addressing vascular complications and restoring blood flow [1–3]. The primary function of stents is physical expansion, which is vital for reopening blood vessels clogged with substances such as cholesterol and plaques [1,4]. However, the physical expansion during the procedure may damage vascular tissue, particularly affecting endothelial cells (ECs), which are crucial for maintaining vascular homeostasis. This cellular impact can trigger events such as inflammation [5,6]. Additionally, mechanical forces applied by stents can induce dedifferentiation of smooth muscle cells within the vessel wall [7,8]. Damaged ECs lose their antithrombotic properties, and dedifferentiated smooth muscle cells (SMCs) contribute to the neointimal hyperplasia characteristic. As a sequence of events, these factors contribute to restenosis, resulting in the recurrence of vessel blockage, posing a problem that may reduce stent implantation's long-term effectiveness [9]. Therefore, it is essential to highlight and understand the complexity and importance of cellular responses to achieve sophisticated stent-based vascular interventions. In pursuing high therapeutic efficacy with minimal side effects, next-generation stents should prioritize goals such as rapid endothelialization and selective inhibition of SMC proliferation. These objectives are crucial for preventing stent restenosis and addressing chronic issues, including persistent inflammation, at various stages of vascular regeneration.

It is well established that cells cultured *in vitro* often lose their inherent characteristics owing to the disparate environment compared to the intricate tissue within the human body [10]. Given the highly complex structure of vascular tissues, the interaction between stents with nonstructural surfaces and the vascular environment may lead to the loss of distinctive properties in adjacent cells. Over the past decade, extensive research has focused on how ECs and SMCs interact with various topographical stimuli to influence vascular cells selectively [11–15]. Metal-based cell culture platforms that replicate the metallic characteristics of NiTi alloys were previously proposed using photolithography and direct current (DC) magnetron sputtering technology [13]. This study demonstrated that the selective modulation of SMC and EC based on various topographies of silicon surfaces exhibiting metallic characteristics is possible, confirming that the micropatterning of vascular cells allows for the selective modulation of cell behavior. Han et al. [14] made a noteworthy contribution by enhancing the biocompatibility of cardiovascular materials. They achieved this by incorporating an extracellular matrix coating and utilizing hyaluronic acid micropatterns to regulate SMC and EC phenotypes, thereby addressing potential clinical complications. Zhou et al. [15] reported surface gradients with diverse nano-to-micrometer roughness on biodegradable metals. This study revealed different cellular reactions, especially in areas with high roughness, highlighting how surface fracturing profoundly influences the biochemical signals to which cells respond. Despite this evolving trend, systematic investigations of the adhesion and proliferation of ECs and SMCs in response to defined surface roughness on clinically relevant implant substrates remain limited, underscoring the need for more in-depth research.

Implants, such as stents, once inserted into the body, are continuously in contact with surrounding tissues and cells. Numerous studies have extensively reported that the surface properties of the implant materials can significantly influence the cellular responses of the surrounding tissues [16]. The emergence and advancement of laser-texturing surface technology have significantly improved the precision, customization, and diversity of surface modifications [17–20]. In particular, the rapid, non-contact, and highly reproducible processing capabilities of medical stent laser cutting are increasing expectations for the precision processing of metal surfaces. Conventional surface texturing methods like sandblasting and chemical etching require masking, hand polishing, or third-party processing, whereas laser texturing streamlines the process by eliminating these steps and offers high reproducibility through precise control over laser parameters, ensuring consistent and repeatable surface patterns under identical processing conditions [21,22]. In this context, we investigated the impact of laser-textured NiTi surfaces featuring nano/microscale wrinkle (nano-W and micro-W) patterns on the fate of endothelial and SMCs. We utilize the precision, customization, and versatility of metal surface modification offered by nanosecond lasers, integral components of laser cutting machines, to investigate the impact of laser-textured NiTi metal surfaces on controlling the fate of endothelial cells (ECs) and smooth muscle cells (SMCs). This involves verifying the differences in their migration based on the specific characteristics of the metal surface topographies. We validated the effectiveness of ECs cultured on the laser-textured surface of NiTi. This validation utilized a co-culturing method with monocytes on the tumor necrosis factor-alpha (TNF-α) treated EC layer. Our exploration delves deeply into the subtle cellular behaviors and molecular interactions that define the response to the stent surface, providing comprehensive insight into the interaction between the microenvironment and metal surface properties. In addition, mouse fetal metatarsal analysis was conducted as an *ex vivo* assessment to examine the influence of metallic surfaces on new blood vessel formation, extending the exploration of endothelialization. We focused on exploring the potential of laser-textured surfaces to influence the complex biological processes crucial for successful stent integration into the vascular environment. Our comprehensive investigation, that connects cell biology and materials science, aimed to provide valuable insights into the constantly evolving field of stent technology. This effort indicates the potential to pioneer innovative advancements aimed at addressing the intricate challenges posed by vascular diseases.

2. Experimental section

2.1. Laser texturing process on NiTi

We used an equiatomic NiTi alloy (biomedical-grade nitinol alloy from Alfa Aesar, Ward Hill, MA, USA) which was cut into 1 × 1 cm plate. These pieces underwent mechanical polishing with 100-, 600-, 1000-, and 2000-grit SiC paper. This process aimed to eliminate contaminants and establish a smooth surface for laser texturing. The control group (pristine, flat) exhibited the dominant phase within the matrix, identified as the B19' phase, and was characterized without any laser texturing to serve as a baseline comparison. A nanosecond ytterbium fiber laser (ytterbium fiber laser, 1064 nm, Laservall), providing a maximum average power of 20 W, pulse duration of 4∼200 ns, and repetition rates of 1.6∼1000 kHz, was employed in this study. For the laser texturing of NiTi, the power was set to 4 W, with a pulse duration of 4 ns, a repetition rate of 800 kHz, and a scan speed of 0.5 m/s. In all laser processes, the laser output was measured using a power meter (Nova II, Ophir, Israel) before irradiating the specimens. The laser beam with a Gaussian profile was focused perpendicularly on the test-piece using an f-theta lens (focal length 160 mm, Jenoptik) and two-dimensional galvanometric mirrors. The spot diameter at the focal point on the test-piece surface was calculated as 32.53 μm by $1/e^2$ using a laser beam quality factor of $M^2 = 1.2$ and a collimated laser beam diameter of 8 mm from the laser. We fixed the parameters of power, pulse duration, and repetition rate to minimize surface damage while achieving the desired nano/micro-scale surface texture with optimal process efficiency. The detailed laser texturing conditions used in this study are provided in the supporting information in Table 1. The laser-textured NiTi was immersed in distilled water for 10 min and then washed twice.

2.2. Characterization of laser-textured NiTi

We performed all analyses of the laser-textured NiTi after completing the laser texturing process and performing thorough sterilization with 70 % ethanol (EtOH) and UV treatment (for 2 h) before conducting cell

experiments. After the ethanol immersion, the samples underwent three washes with phosphate-buffered saline (PBS) to remove residual ethanol. The surface roughness induced by laser texturing of the samples was evaluated at 0° and 13° tilts using scanning electron microscopy (SEM) with a high voltage (HV) of 15 kV, spot size of 3.0–3.5 nm, and working distance (WD) of 9.6–27.8 mm. The patterned surface roughness (Ra) was quantified and characterized using atomic force microscopy (XE-100, Park Systems). Samples were scanned at the repetition rate of 0.4 Hz in the non-contact mode on a 15 × 15 μm^2 surface area using a non-contact cantilever (PPP-NCHR, Park System). Ra was used to analyze the surface roughness, representing the arithmetic average of the absolute values of the profile height deviations from the mean line. Cross-sectioned transmission electron microscope (TEM) lamella samples were meticulously crafted using focused ion beam (Helios NanoLab 600, FEI) to scrutinize the intricate, multilayered cross-sectional structure induced by the laser beam. Platinum (Pt) was deposited to protect the surface of the samples. Then, the sample was roughly milled using gallium (Ga^+) ions at 30 keV, and finely milled at 5 keV to avoid forming an amorphous layer on the lamella surface. The final lamella size was approximately 4–5 μm. Nanoscale analyses were performed with a TEM (Talos F200X, FEI) equipped with EDS featuring four silicon drift detectors. The phase evolution beneath the surface was characterized by electron diffraction patterns determining the crystal structure and energy-dispersive spectroscopy (EDS) quantifying the chemical composition in TEM. To elucidate the crystal structure, based on the size of the area for each phase, we acquired selected area electron diffraction (SAED) patterns, nano beam diffraction (NBD) patterns, or Fast Fourier Transform (FFT) patterns. In cases where the size was larger than 200 nm, we employed SAED patterns using a selected area aperture in TEM. For sizes smaller than 5 nm, mathematically obtained FFT patterns were used. In the intermediate size range, NBD patterns with a focused electron beam were obtained. The static water contact angles on the laser-textured NiTi surfaces were measured using the sessile drop method with a contact angle meter (Digi Drop, DGD, Fast/60, GBX, France) by depositing a 5 μL droplet of deionized water onto the dry surface of each laser-textured NiTi membrane for 60 s. Images of the droplet were captured using a charge-coupled device camera, and the mean contact angles were calculated using NIH ImageJ medical imaging software version 1.54 (http://rsbweb.nih.gov/ij/, National Institutes of Health, Bethesda, MD, USA). For all cell analyses, cells were directly cultured on laser-textured NiTi surfaces without any protein coating. However, to explore the impact of controlled protein adsorption on cell behavior, we also explicitly coated the laser-textured NiTi surfaces with fibronectin, one of the major extracellular matrix (ECM) proteins, to study its influence on protein adsorption. Laser-textured NiTi (1 × 1 cm) samples were incubated in 2 mL fibronectin solution (2 μg/mL in PBS buffer) for 2 h at room temperature with mild shaking. The remaining fibronectin in the supernatant was measured using a microplate reader (Tecan, Männedorf, Switzerland) at 562 nm, following the MicroBCA Protein Assay Kit protocol, to calculate the amount of adsorbed protein. To verify the presence of fibronectin on the laser-textured surfaces, we used FITC-conjugated anti-human fibronectin antibody for immunostaining and observed the samples using a confocal microscope (LSM 700, Carl Zeiss). The microstructural characteristics of laser-textured NiTi were acquired using X-ray diffraction (XRD; D/MAX-2500, Rigaku, Tokyo, Japan). Different phases in samples were identified using XRD with CuKα radiation. Measurements were conducted in the 2θ range from 20° to 60° with a step size of 0.02° and a scan speed of 2°/min.

2.3. Cell culture

ECs (human umbilical vein endothelial cells) and SMCs (human aortic smooth muscle cells) were obtained from Lonza and cultured in specialized growth media tailored for ECs (Lonza endothelial growth medium [EGM]-2, USA) and SMCs (Lonza smooth muscle growth medium-2, USA), respectively. Both cell types were maintained under standard cell culture conditions (37 °C, 5 % CO_2). Passages were performed at 70%–80 % confluence using ACCUTASE™ Cell Detachment Solution (Thermo Fisher Scientific, Germany), and the cells were then seeded on laser-textured NiTi surfaces. Both cell types were used for all experiments between passages four and six.

2.4. Analysis of adherent vascular cells on laser-textured NiTi surfaces

To examine the adhered cells on laser-textured NiTi, both cell types were seeded onto each laser-textured NiTi sample at a density of 1 × 10^4 cells/cm^2 and cultured in EGM-2 for ECs and smooth muscle growth medium-2 for SMCs 24 h. Vascular cells on laser-textured NiTi were fixed with 4 % paraformaldehyde and permeabilized in a cytoskeleton buffer (0.5 % Triton X-100). After permeabilization, the laser-textured NiTi surfaces were blocked by incubating with 2 % fetal bovine serum and 0.1 % Tween-20 in phosphate-buffered saline, followed by sequential incubation with anti-paxillin, anti-mouse IgG biotin conjugate, and fluorescein isothiocyanate (FITC)-conjugated streptavidin (Thermo Fisher Scientific, Germany). The cytoskeletal structure and nuclei were counterstained with rhodamine-phalloidin and 4′,6-diamidino-2-phenylindole (DAPI), respectively. Adherent cells were visualized under a confocal laser scanning microscope (LSM 700; Carl Zeiss, Oberkochen, Germany). Subsequently, the nuclei count projected adherent cell area and orientation angle of the adherent cells were quantified by analyzing the DAPI-stained images using the ImageJ medical imaging software (NIH). The nuclei aspect ratio was determined by dividing the short axis (width) by the long axis (length) at the same magnification. Cell proliferation on the laser-textured NiTi was evaluated using 5-bromo-2′-deoxyuridine (BrdU) incorporation staining. Briefly, 24 h after seeding on the laser-textured NiTi, the cells were replenished with growth media containing BrdU (10 μM) and incubated for an additional 3 h. Following this, cells were fixed with 4 % paraformaldehyde for 20 min and treated with 2N hydrochloric acid for 30 min. After blocking with 10 % fetal bovine serum for 1 h at 37 °C, cells were sequentially incubated with anti-BrdU antibody, anti-mouse IgG biotin conjugate (Sigma), and FITC-conjugated streptavidin (eBioscience, San Diego, CA). BrdU-positive nuclei were quantified using ImageJ software (NIH).

2.5. Evaluation of vascular cell functionality on laser-textured NiTi

For the immunostaining of ECs, the cells were subjected to fixation, permeabilization, and subsequent incubation with anti-platelet endothelial cell adhesion molecule (PECAM, Thermo Fisher Scientific, Germany), anti-von Willebrand Factor (vWF, Thermo Fisher Scientific, Germany), and anti-Tyrosine Kinase with Immunoglobulin-like and EGF-like Domains 2 (Tie-2) antibodies. Subsequently, they were treated with an anti-mouse IgG biotin conjugate and FITC-conjugated streptavidin before visualization using confocal laser scanning microscopy (LSM 700, Carl Zeiss, Germany). Similarly, for the immunostaining of SMCs, the cells were fixed, permeabilized, and incubated with anti-matrix metalloproteinase (MMP)-2 and anti-collagen III antibodies. The cells were then exposed to an anti-mouse IgG biotin conjugate and FITC-conjugated streptavidin and visualized using confocal laser scanning microscopy. According to the manufacturer's instructions, the total RNA from each cell culture on the laser-textured NiTi surfaces was extracted using a column-based kit (RNeasy Plus mini kit; Qiagen, Hilden, Germany); it was then concentrated, purified, and used for complementary DNA synthesis using the Maxime RT Premix Kit (Intron Biotechnology, Korea). Real-time reverse transcription polymerase chain reaction (RT-PCR) data were analyzed using the comparative threshold cycle method. The relative expression of each gene was calculated by comparing it with the expression level of β-actin and subsequently normalized to the value for cells cultured on the control (untreated NiTi). The oligonucleotide primer sequences are listed in Supporting information Table 3. Real-time RT-PCR using SYBR green

master mix was conducted using an AB 7500 sequence detection system (Applied Biosystems, Foster City, CA, USA) (40 cycles, melting at 95 °C for 15 s, annealing and extension at 60 °C for 60 s).

2.6. Migration assay

Fluorescent images were obtained to investigate the migration of cells on laser-textured NiTi. Briefly, vascular cells were seeded (1×10^5 cell/cm^2) onto the surface of the laser-textured NiTi featuring a strategically positioned barrier (polydimethylsiloxane mold, circular diameter of 8 mm) that impeded cell adhesion to the central region of each well. The cells were fluorescently labeled with DiO-fluorescent dye (green signal) at 72 h, and low-magnification (10 ×) tile scan images were produced using confocal imaging on a Carl Zeiss imaging system (Carl Zeiss, Germany). The distribution of migrated cells was quantified by analyzing DiO-labeled cell images using ImageJ software (NIH).

2.7. Monocyte adhesion assay

The THP-1 human acute monocytic leukemia cell line was obtained from the American Type Culture Collection and cultured in RPMI 1640 medium supplemented with 10 % fetal bovine serum and 1 % penicillin-streptomycin. THP-1 cells were cultured to confluency on a tissue culture plate under growth medium, then the Vybrant DiO solution (Molecular Probes, OR, USA) was added at a concentration of 5 μL/mL (1:200) and incubated at 37 °C for 2 h, subsequently washed twice with fresh medium. After forming an EC monolayer on the laser-textured NiTi surfaces, 10 ng/mL of TNF-α (Sigma–Aldrich, MO, USA) diluted with EGM-2 medium was applied to the EC layer for 12 h. Following TNF-α stimulation, Vybrant DiO solution-labeled THP-1 monocytes at a density of 2.5×10^4 cells/cm^2 were subsequently co-cultured on the EC layer on laser-textured NiTi. To assess the captured THP-1 monocytes in the EC layer, DiO-labeled THP-1 cells were transferred to the EGM-2 medium and spread on the TNF-α-stimulated EC monolayer for 45 min with gentle shaking. After monocyte adhesion, the laser-textured NiTi surfaces were washed twice with PBS to remove the unbound monocytes. The number of adherent monocytes on the EC layer was calculated by counting the DiO labeling signals using ImageJ software (NIH).

2.8. Fetal mouse metatarsal angiogenesis assay

We verified the angiogenesis required for the rapid endothelialization of damaged vascular walls through *ex vivo* testing on NiTi surfaces. The fetal metatarsal angiogenesis assays were performed in accordance with the relevant guidelines and regulations of the Institutional Animal Care and Use Committee (IACUC) and the Institutional Biosafety Committee (IBC) at KIST (Approval number KIST-IACUC-2023-043-1). Briefly, fetal mouse metatarsals were obtained from E17.5 embryos of CD1 mice. The feet were carefully dissected immediately above the ankle joint of the fetus using a dissection stereomicroscope (Olympus, Japan). The dissected metatarsals were meticulously transferred to a fresh 10-cm culture dish containing an ice-cold dissection medium using tweezers. One pair of tweezers was inserted between the skin and the calcaneus, while the other pair held the exposed fibula. The first pair of tweezers was gently advanced into the footpad while removing the skin and phalanges, leaving the tarsals and metatarsals intact. Excessive connective tissue attached to the metatarsals was removed, and the metatarsals were separated. Only the middle three metatarsals were retained, and the first and fifth metatarsals were discarded. The isolated metatarsals were then cultured on laser-textured NiTi surfaces in alpha-modified Eagle's minimum essential medium (α-MEM) supplemented with 10 % heat-inactivated fetal bovine serum (FBS), 1 % penicillin/streptomycin, and 2 mM L-glutamine for 5 days. During this period, the medium was refreshed every two days to maintain optimal nutrient and growth conditions. After 5 days of culture, the metatarsals were carefully fixed with 4 % paraformaldehyde (PFA) for 20 min at room temperature to preserve cellular and structural integrity. Following fixation, the samples were washed three times with PBS to remove residual fixative. After which, they were fixed and stained with an FITC-conjugated CD31 antibody. Confocal laser scanning microscopy (LSM 700, Carl Zeiss, Oberkochen, Germany) was used to capture high-resolution images of the stained metatarsals. The images were subsequently analyzed and quantified using the Wimasis Angiogenesis Analysis Platform (WIMASIS GmbH, Munich, Germany) to assess angiogenesis, including vessel density and branching.

3. Results and discussion

This study employed nanosecond laser technology, renowned for achieving a practical compromise between high-precision microfabrication and relatively low thermal impacts compared to continuous wave (CW) lasers, through careful adjustment of laser parameters [23]. Nanosecond lasers, characterized by altered time intervals in the nanosecond range (1 ns = 10^{-9} s), play a pivotal role in surface modification in various industrial applications [18,24,25]. Our study aimed to develop a practical method for surface modification of NiTi alloys using laser texturing technology, with a focus on demonstrating that the behavior of vascular cells can be influenced by the roughness of several hundred nanometers generated through the application of a nanosecond laser to the metal surface (Fig. 1).

3.1. Characterization of laser-textured NiTi

We prepared NiTi with wrinkle-like structures via laser texturing, an efficient and accessible method for creating surface patterns on materials. It is well known that wrinkles on laser-textured metal surfaces, formed due to rapid localized heating and cooling induced by nanosecond laser pulses, exhibit varying morphologies depending on factors such as pulse duration, energy density, and the inherent properties of the material [26]. The formation of these wrinkle structures is governed by a complex interplay of mechanisms that occur during and immediately after the application of the laser pulses. When intense laser energy is applied to the metal surface, it rapidly heats and melts a thin surface layer of the metal. This molten layer is influenced by various forces, including evaporation-induced recoil pressure, which pushes material away from the surface, and Marangoni flow, driven by temperature gradients that create surface tension variations [27,28]. These forces create wave-like patterns in the liquid state, which can accumulate and solidify into wrinkles on the surface. As the laser pulse ends, rapid cooling and solidification occur. This quick transition from liquid to solid, combined with the uneven distribution of forces and material during the molten state, has been reported to lead to the formation of nano/micro-scale wrinkles [26–28]. These studies emphasize that surface structuring is not merely a result of thermal effects but also involves dynamic material redistribution under the influence of multiple physical forces during laser processing. This study adjusted laser processing parameters such as the repetition rate and intervals to fabricate nanoscale or microscale wrinkles on NiTi surfaces (Supporting Information S1). During the preliminary phase, the focus was on selecting optimal laser processing conditions for the NiTi surface to create a laser-textured environment that effectively controlled vascular cells (Supporting Information S2-3).The roughness of the flat surface used as a control group was confirmed to be 5.87 ± 1.04 nm Ra. As highlighted in the images of Fig. 2a–c and Supporting Information S4, a faint pattern resembling nano-W emerged on the surface after a single laser texturing process, with a Ra value of 80.20 ± 23.06 nm. The surface roughness for the group subjected to 16 laser-texturing scans increased, resulting in micro-Ws with a Ra of 839 ± 94.75 nm. Furthermore, we precisely controlled the spacing between the nano-W and micro-W patterns, as well as another set of wrinkle patterns, maintaining intervals of 30.27 ± 1.23 μm. This deliberate arrangement aimed to induce the alignment of attached cells. The respective groups were labeled as the patterned

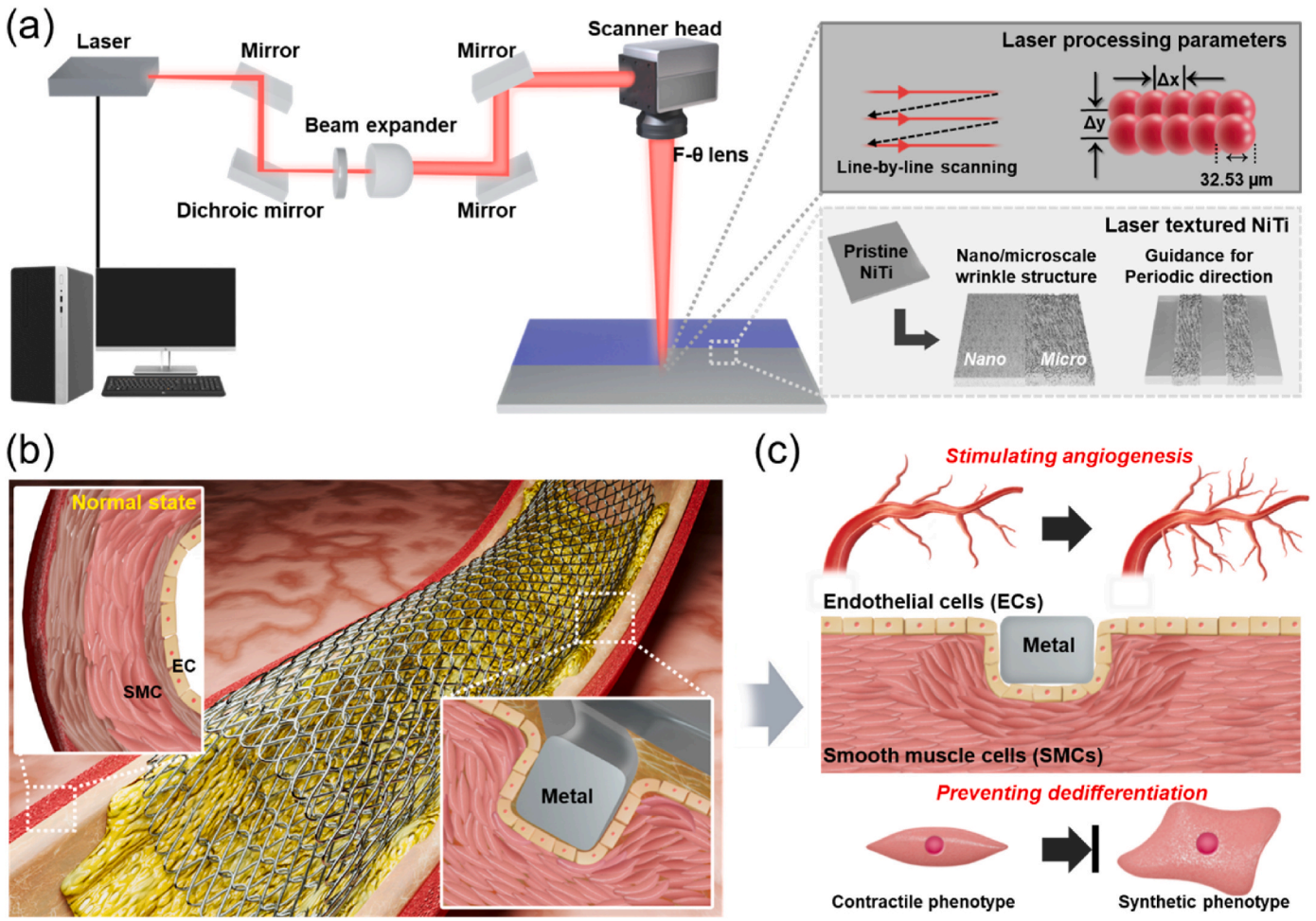

Fig. 1. (a) Schematic illustration shows the setup of a nanosecond laser system used for texturing NiTi surfaces. The inset details the laser processing parameters, depicting the line-by-line scanning approach focusing on the critical dimensions (Δx (spot overlap ratio), Δy (line overlap ratio), and the laser spot diameter) that determine texture resolution. Depending on the laser processing conditions, it is possible to create nano/micro-structured wrinkle patterns or control periodic pattern structures that can influence the orientation of attached cells. (b) The representative images visualize an expanded stent deployed within a blood vessel to re-open clogged blood vessels. The left inset highlights the normal state of a blood vessel with an endothelial cell (EC) lining and a smooth muscle cell (SMC) layer beneath. The right lower inset showcases the vessel wall anchored by the expanded stent, pressing against the endothelial cells (EC) and smooth muscle cells (SMC) layers. (c) The image suggests the multi-functionality of the laser-textured NiTi surface, which can minimize the potential risk of restenosis by promoting angiogenesis for endothelial healing and preventing the dedifferentiation of smooth muscle cells. This design helps the laser-textured NiTi surface effectively interact with ECs and SMCs, providing an environment that promotes desirable cellular responses such as enhanced endothelialization and reduced SMC dedifferentiation.

nano-W (pNW) and patterned micro-W (pMW) groups. The contact angle varied considerably based on the surface characteristics of the laser-textured NiTi (Fig. 2e), with changes in the contact angle affecting protein adsorption. We noted an increase in protein adsorption in the nano-W group and a decrease in the micro-W group compared to the control group (Fig. 2f). Material wettability, widely known to be significantly influenced by surface energy, is mainly affected by the various spatial structures and differences in surface roughness of laser-textured substances [3]. The nano-W patterns likely created a surface with higher energy and more sites for protein attachment, increasing protein adsorption. Conversely, the micro-W patterns might have led to a less energetically favorable surface for protein binding, thus decreasing protein adsorption. Abnormally excessive adsorption of proteins, such as albumin and fibronectin on implanted materials post-implantation can lead to adverse effects like increased infection risk, inflammation, and impaired tissue integration [29,30]. Studies suggest that elevated immune responses triggered by increased protein adsorption contribute to implant rejection and negatively affect the overall success of implantation. Our findings indicate that laser-textured NiTi with micro-W may provide an advantageous environment that overcomes the drawbacks caused by material-protein interactions after implantation.

Fig. 2g illustrates the use of X-ray diffraction to investigate changes in the TiO_2 crystal phase of NiTi due to laser texturing. We confirmed the formation of multiple oxide layers (rutile and anatase) through repetitive laser texturing (pMW group). Anatase and rutile are two distinct titanium dioxide (TiO_2) crystal structures that manifest in the solid state [31]. Anatase TiO_2 features a body-centered tetragonal crystal system with atoms arranged within slightly distorted octahedra, differing from rutile TiO_2, which also adopts a tetragonal crystal system but is characterized by a more compact and elongated octahedral configuration of atoms [32]. These differences in crystal structure significantly influence their bonding with oxygen, contributing to their unique properties among the various forms of titanium used in materials science [33]. We conducted a detailed exploration of the crystallographic characteristics and nanoscale features of the laser-textured NiTi using TEM, as shown in Fig. 2h. The NiTi alloy known for its biocompatible properties [34] exhibits a unique ability to reversibly transform between austenitic and martensitic phases, making it highly suitable for manufacturing of stent-shaped structures. The control group (pristine, flat) predominantly exhibited the B19′ phase within the matrix, which is recognized for its thermodynamic stability at room temperature due to the high

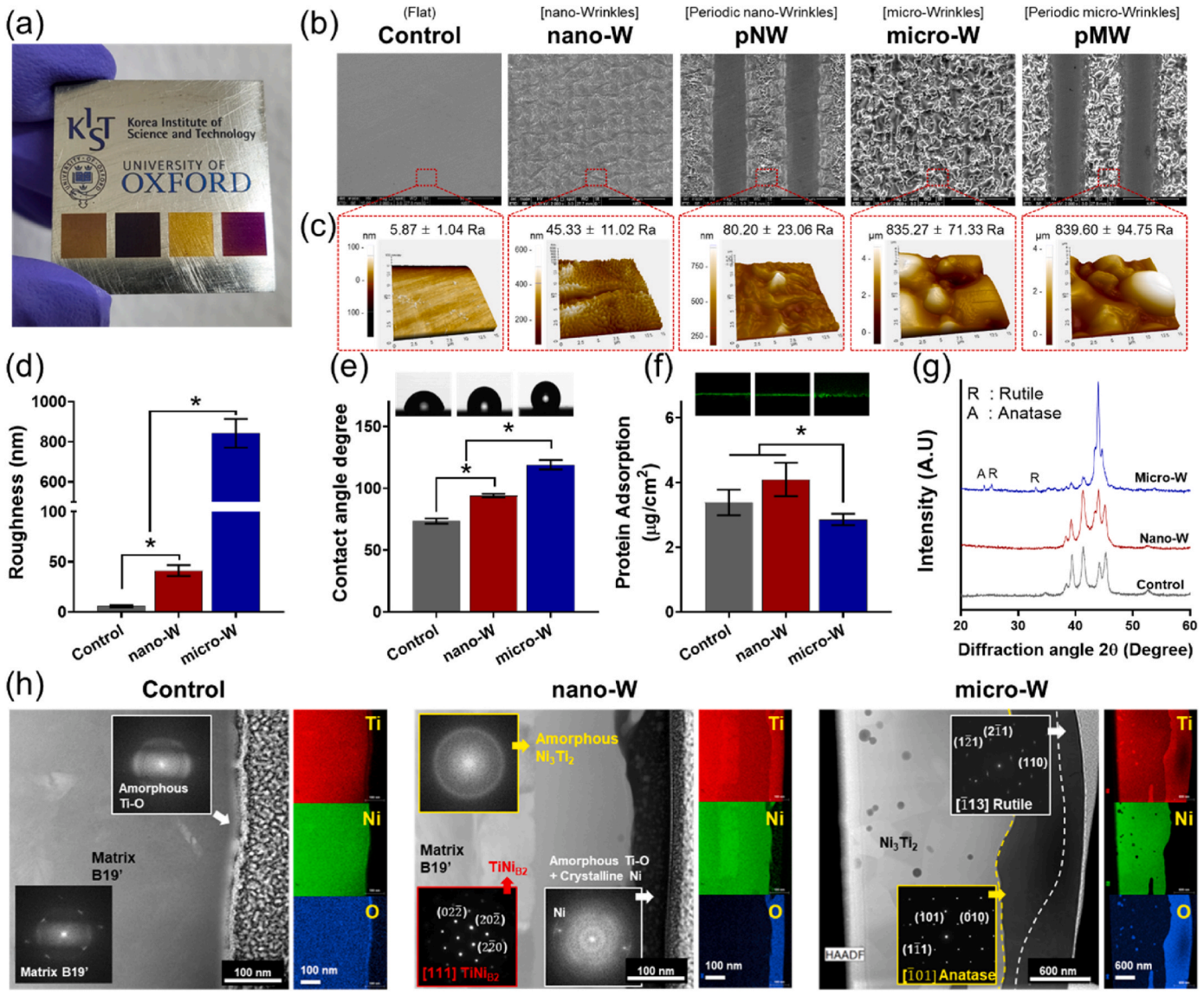

Fig. 2. (a) a bright-field image highlights the surface texturing of NiTi achieved through laser processing. Representative SEM (Scanning Electron Microscopy) and AFM (Atomic Force Microscopy) images in (b) and (c), respectively, offer detailed insights into the morphological characteristics of laser-textured NiTi. Quantitative analyses of (d) surface roughness, (e) contact angle, and (f) protein adsorption of laser-textured NiTi, highlighting depending on processing conditions. Figure (g) presents an XRD (X-ray Diffraction) analysis, providing insights into the structural characteristics of laser-textured NiTi. Lastly, (h) showcases a HAADF STEM (High-Angle Annular Dark-Field Scanning Transmission Electron Microscopy) image accompanied by diffraction patterns showing crystal structure and EDS (Energy-Dispersive X-ray Spectroscopy) elemental maps, illustrating the elemental distribution of Ti (red), Ni (green), and O (blue) in laser-textured NiTi with high resolution. * indicates significant difference ($p < 0.05$, $n = 3$).

martensite start temperature inherent in equiatomic NiTi alloys [35]. Following the single-laser texturing process (nano-W), the surface underwent a notable transformation. For instance, in the case of nano-W, the outermost thin surface layer exhibited an amorphous ring with distinct spots in FFT pattern (Supporting information S5), which were indexed as Ni. The quantitative composition of this layer was determined to be 49.14 % Ti, 5.80 % Ni, and 45.06 % O (Supporting information Table 2). Therefore, we concluded that it consisted of Ni nanocrystals embedded within an amorphous TiO matrix. Repeated laser texturing of NiTi, as in the micro-W group, formed a thicker oxide layer of about 600 nm encompassing multiple oxide layers, including rutile and anatase. Notably, both anatase and rutile phases formed under our laser texturing conditions, with a high repetition rate of 800 kHz and sufficient power of 4 W [36]. The coexistence of rutile and anatase layers is comparable to conventional heat treatment methods used to control the surface crystal structure of NiTi (Supporting Information S6). Under heat treatment in air, the crystal structure of the NiTi surface transitions first to the anatase phase and subsequently to the rutile phase, as reported in the literature [37]. The surplus Ni atoms persisting within anatase TiO_2 following iterative laser texturing instigated a noteworthy phase transition from anatase to rutile. This surplus of Ni atoms seamlessly integrates into the Ti sublattice of the anatase phase, creating oxygen vacancies and ultimately dictating the transformation from anatase to rutile [36]. We propose that laser-texturing technology offers a feasible alternative for managing the crystal structure of the NiTi surface, providing the advantage of precisely adjusting the metal surface characteristics to optimize interactions with the biological environment. Subsequently, the efficacy of laser texturing technology lies in its capacity to tailor the surface properties of NiTi to specific requirements, thereby enhancing its suitability for various biomedical applications.

3.2. Exploring cellular morphology and functional behavior on laser-textured NiTi

Topography plays a crucial role in influencing the behavior and function of cells, as various surface structures have been reported to enable controllable regulation of ECs and SMCs, such as proliferation and differentiation [8,12,38]. The investigation aimed to assess how the communication between the topographies on laser-textured NiTi and vascular cells influenced their morphologies and function. As shown in Fig. 3a, the ECs cultured on laser-textured NiTi exhibited consistent focal adhesion protein expression in all groups. Notably, ECs cultured on laser-textured NiTi with directionally pMW groups showed an orientation within 20 degrees of the long axis (>80 %) compared to other groups (Supporting Information S7). However, no notable differences were observed in the projected cell area and proliferation among the groups (Fig. 2c and d and Supporting Information S8). For example, in the quantification analysis of BrdU-positive nuclei in ECs, it was 24.59 ± 1.36, 24.07 ± 1.57, 25.03 ± 1.76, 23.06 ± 3.27 and 24.85 ± 2.90 % for control, nano-W, pNW, micro-W and pMW, respectively.

In contrast to ECs, as shown in Fig. 3b, the adherent morphologies of SMCs cultured on laser-textured NiTi exhibited significant differences between the groups with defined topographical patterns. We examined the expression of focal adhesion proteins in muscle cells cultured on flat surfaces (controls). In contrast, SMCs cultured on NiTi surfaces featuring nano-W and micro-W patterns exhibited a decrease in the signal of focal adhesion proteins. We noted distinct changes in the morphology of the attached cells, especially in laser-textured NiTi with micro-W and pMW features compared to the control. In addition, we found that the mean projected cell areas from the micro-W and pMW groups were smaller than those from the control group (Fig. 2e). The projected cell area of SMCs showed 13434.37 ± 4664.19, 11096.58 ± 2923.35, 11109.07 ± 2710.23, 6811.50 ± 2270.95 and 7732.81 ± 2469.54 μm^2 for control, nano-W, pNW, micro-W, and pMW, respectively. The adherent cells in the pMW group also showed an orientation within 10° of the long axis compared to the control group (Supporting Information S9). Consistent with the proliferation results (Supporting Information S10), BrdU-incorporated nuclei significantly decreased in groups characterized by micro-W structures compared to the control and nano-W groups (Fig. 2f). For example, in the quantification analysis of BrdU-positive nuclei in SMCs, values were 32.75 ± 3.92, 26.93 ± 3.24, 25.73 ± 4.71, 10.27 ± 2.09 and 9.73 ± 4.90 % for control, nano-W, pNW, micro-W and pMW, respectively. These results suggest SMCs exhibit higher reactivity at the cell-material interface than ECs.

Promoting swift healing of injured endothelial tissue is essential for averting the adverse consequences of in-stent restenosis [39]. Facilitating rapid recovery involves encouraging quick restoration of damaged ECs, which is a critical step in preventing complications associated with the narrowing of blood vessels after stent insertion [39]. The expression of key EC proteins, such as PECAM, Tie-2, and vWF, plays a central role in promoting swift re-endothelialization [40,41]. These proteins contribute significantly to cell attachment, communication, and overall vascular integrity, creating a favorable environment for EC proliferation and restoring a functional endothelial layer, emphasizing their importance. To assess whether cell function was influenced by interactions with the topographies of laser-textured NiTi, ECs were cultured on laser-textured NiTi groups for 5 days. In Fig. 4a, representative immunofluorescence images depict green fluorescence representing PECAM and vWF, which are pivotal in promoting swift re-endothelialization. Over an extended culture period (5 days) compared to the short term (24 h), the pNW and pMW groups revealed the directional alignment of actin filaments in the cultured vascular cells. The PECAM protein was distributed at the intracellular junctions of ECs in all the laser-textured NiTi groups. The pMW group exhibited higher vWF protein expression than the other groups. Gene expression analysis of ECs showed similar or higher expression for cells in groups with specific topographies than those cultured in the control group

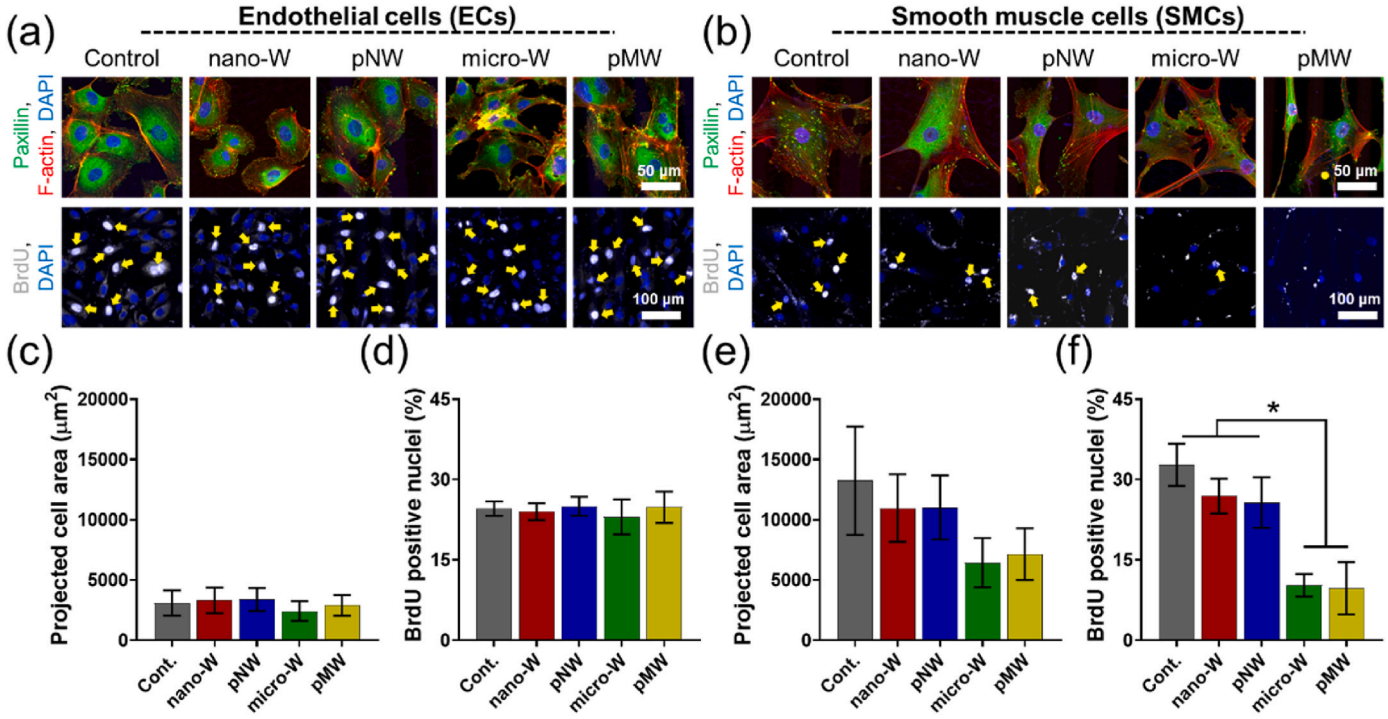

Fig. 3. Cytoskeletal structures, focal adhesion distributions, and BrdU-incorporated nuclei were examined in (a) human smooth muscle cells (SMCs) and (b) human endothelial cells (ECs) after 24 h of culture on laser-textured NiTi substrates. The images were acquired through immunofluorescence staining for paxillin (green), F-actin (red), BrdU (white), and DAPI (nuclei). (c) Quantification of the projected area of endothelial cells on laser-textured NiTi. (d) Percentage of BrdU-positive nuclei in endothelial cells cultured on laser-textured NiTi. (e) Quantification of the projected area of smooth muscle cells on laser-textured NiTi. (f) Percentage of BrdU-positive nuclei in smooth muscle cells cultured on laser-textured NiTi. * indicates a significant difference ($p < 0.05$, $n = 5$).

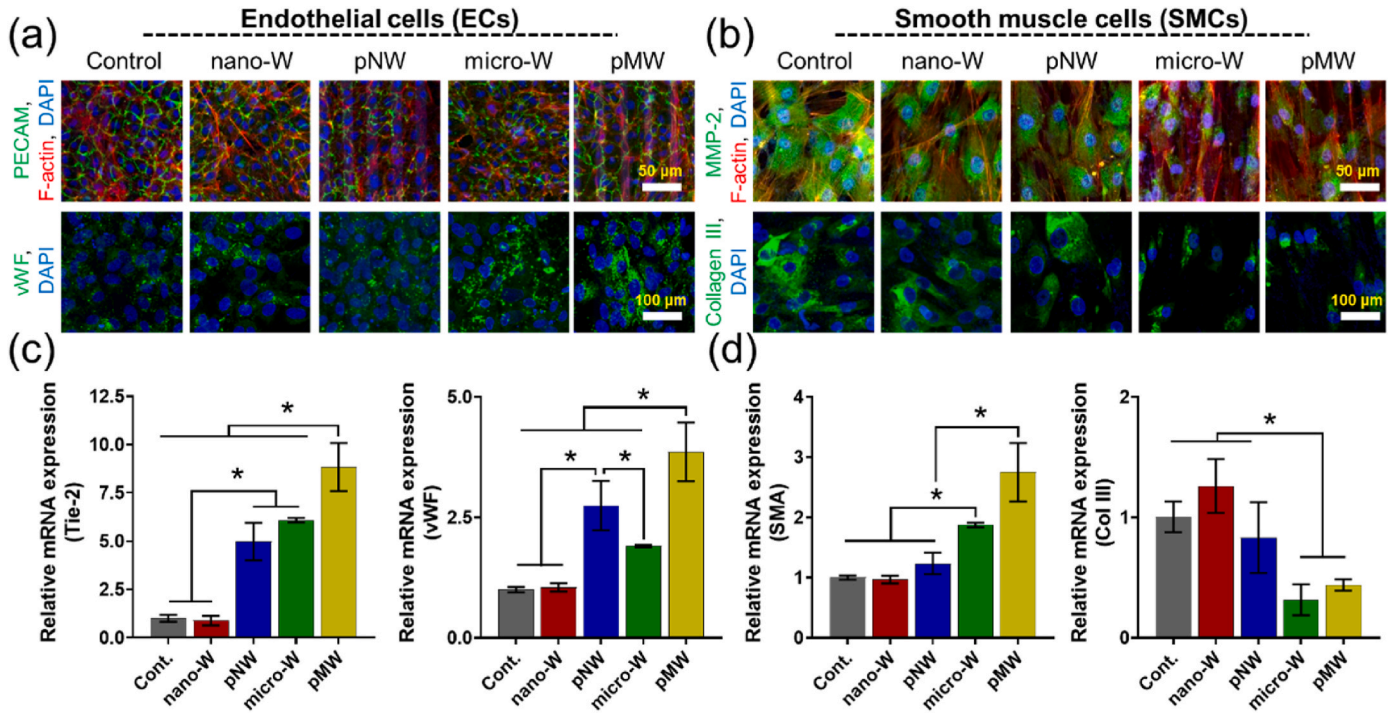

Fig. 4. (a) After a 5-day culture, ECs on laser-textured NiTi substrates were stained for PECAM and vWF. (b) SMCs cultured on laser-textured NiTi substrates for 5 days were subjected to staining for MMP-2 and Collagen III. The relative expression levels of genes in ECs cultured on laser-textured NiTi for 5 days were examined. (c) Quantification analysis was performed using real-time RT-PCR for Tie-2 and von Willebrand factor (vWF). (d) The relative expression levels of genes in SMCs cultured on laser-textured NiTi for 5 days were analyzed. This involved quantification through real-time RT-PCR for α-SMA and Col III. * indicates a significant difference ($p < 0.05$, $n = 5$).

(Fig. 4c). The expression levels of the Tie-2 gene demonstrated a notable increase on laser-textured NiTi: 4.98 ± 0.98-fold on pNW, 6.08 ± 0.11-fold on micro-W, and 8.83 ± 1.24-fold on pMW, in comparison to the control (Flat). However, Tie-2 gene expression levels on nano-W (0.88 ± 0.24-fold) were comparable to the control.

SMCs in their normal state exhibit high expression of smooth muscle alpha-actin (α-SMA), contributing to the contractility and maintenance of the phenotype of these cells [7]. Conversely, abnormal proliferation and differentiation are observed when SMCs enter a dedifferentiated state, a response alteration caused by the increased secretion of MMP [42–44]. This leads to a disorganized extracellular matrix (ECM), supporting the dedifferentiated phenotype of SMCs. Persistent dedifferentiation, marked by increased collagen III deposition, disrupts normal cell-matrix interactions and promotes pathological vascular remodeling, resulting in excessive SMC infiltration, neointimal hyperplasia, vascular integrity disruption, and lumen narrowing, commonly leading to diseases such as atherosclerosis, restenosis, and vascular stenosis. Fig. 4b displays representative immunofluorescence images, where the green fluorescence corresponds to MMP-2 and Collagen III. Fluorescence imaging and gene expression analysis revealed that SMCs cultured in the micro-W and pMW groups exhibited a notable reduction in collagen III deposits compared to the other groups (Fig. 4b and d). The down-regulation of secretory phenotypes, indicative of dedifferentiation, was notably more pronounced in laser-textured NiTi with micro-W topographies than in the other groups. In Fig. 4d, the expression of α-SMA was higher on NiTi with micro-W topographies than on all other groups. However, the signal from MMP-14, a dedifferentiation marker for SMCs, was diminished in cells cultured on nano-W (1.26. ± 0.22), pNW (0.83 ± 0.29), micro-W (0.32 ± 0.13), and pMW (0.43 ± 0.05) to those cultured on control (1.00 ± 0.12) (Supporting information S12). These findings suggest that the laser-texturing technique on NiTi alloy can provide a controlled environment conducive to endothelialization in ECs and effectively manage the dedifferentiation of SMCs. This effect is attributed to the mechanical and chemical properties induced by laser texturing, where topographical features improve cell adhesion, spreading, and alignment, and chemical changes reduce protein adsorption and inflammation. Specifically, with its carefully designed micro-W and nano-W patterns, the laser-texturing technique is pivotal for creating a surface that facilitates a favorable environment for EC culture. These patterns contribute to a controlled microenvironment, promoting cellular responses by providing cues for EC attachment and growth while mitigating the undesirable dedifferentiation process in SMC. Our results underscore the potential of this laser-texturing technology to modulate cellular behavior precisely, highlighting its applicability in steering the re-endothelialization process and preventing the detrimental effects associated with SMC dedifferentiation.

3.3. Cell migration on laser-textured NiTi surfaces

Cell migration catalyzes tissue healing and angiogenesis, thereby promoting endothelization [8,45]. Conversely, preventing the excessive proliferation of SMCs, which is the leading cause of restenosis after stent insertion, is one of the essential factors in preventing restenosis [6,7]. We examined whether laser-textured NiTi surfaces could modulate vascular cell migration. As depicted in Fig. 5 and Supporting Information S14, ECs on laser-textured NiTi with defined topographies exhibited a coverage of migrated cells comparable to those on a flat surface (as a control). For instance, the control group showed 62.79 ± 6.39 %, and the micro-W group exhibited a 59.15 ± 1.77 % migrated cell area (Fig. 5d). In contrast, SMC migration extensively covered the entire area of the control, nano-W-, and pNW groups. However, for micro-W and pMW, there was a noticeable reduction in the coverage of the migrated SMCs. A quantification analysis revealed a significant difference in the migrated area of cells/mm^2: control (97.33 ± 2.94 %), nano-W (92.77 ± 1.28 %), pNW (98.18 ± 2.28 %), micro-W (75.89 ± 2.52 %), and pMW (75.75 ± 3.15 %). These results indicate that SMCs possess better migratory capabilities than ECs in the same environment. Consistent with previous findings, ECs cultured on laser-textured NiTi with defined

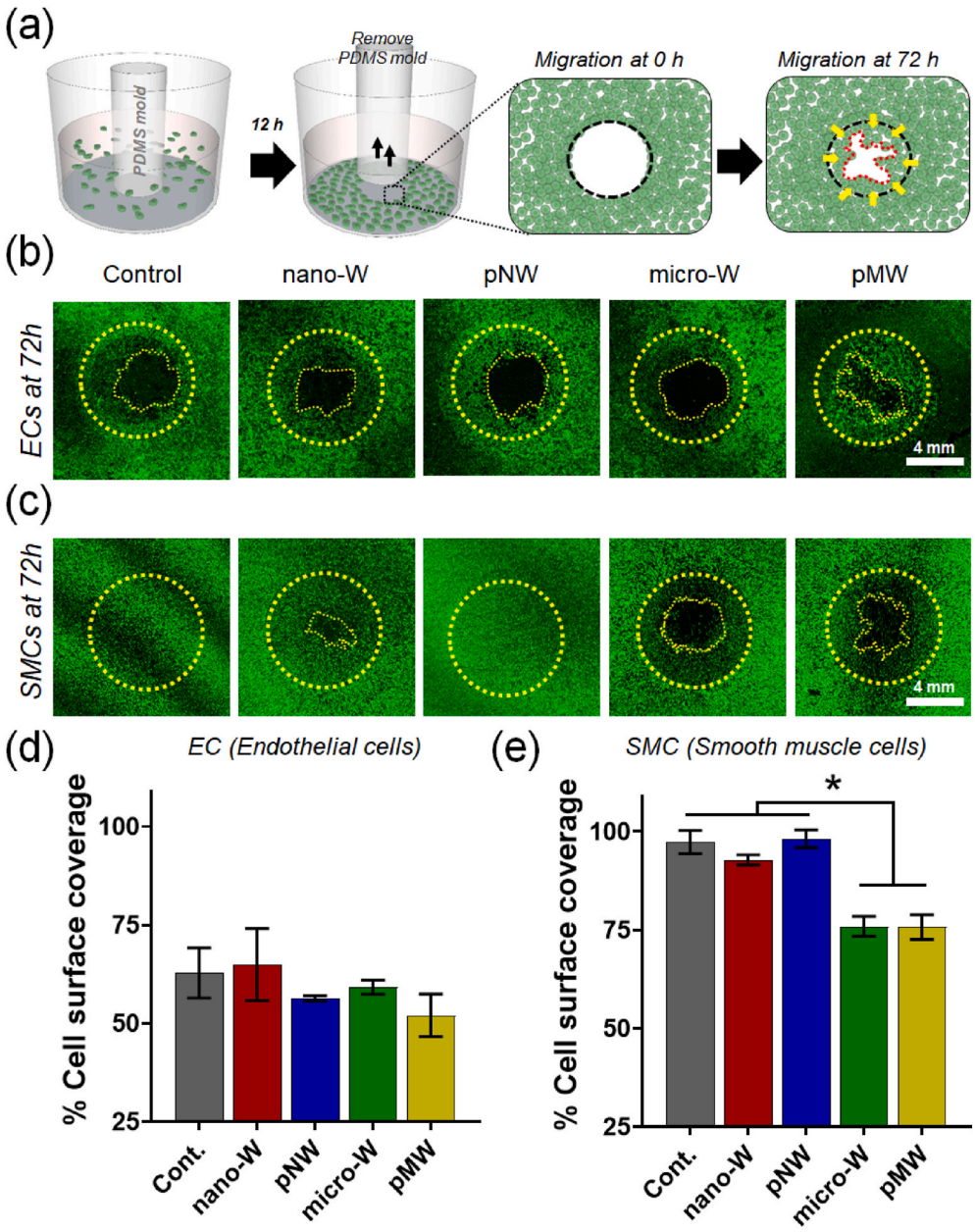

Fig. 5. (a) The schematic depicts an approach to analyzing cell migration on laser-textured NiTi. Vascular cells are applied onto the surface of laser-textured NiTi, featuring a strategically positioned barrier (PDMS mold) that impedes cell adhesion to the central region of each well. After 12 h, the barrier is removed, revealing a distinct vacant space at the center of the well. Over a 72-h incubation period, the movement of fluorescent DiO-labeled (b) ECs and (c) SMC that migrated into the central zone was monitored. Quantitative analysis of cell surface coverage (%) for (d) EC and (e) SMCs that migrated to the center. * indicates a significant difference ($p < 0.05$, $n = 4$).

topographies demonstrated comparable or enhanced cellular functionality and behavior compared to the control. In contrast, SMCs appear to be more strongly influenced by the size and topographic features of the material surface. These results were attributed to the structural characteristics of the NiTi surface following laser texturing and the differences in the altered crystalline phases. Suzuki et al. explored the effect of nano-scale TiO_2 particles with distinct crystalline structures (anatase and rutile) on arterial atherosclerosis [46]. The findings revealed an increased area of arterial atherosclerosis in the arteries of ApoE−/− mice exposed to anatase TiO_2 phase, while rutile TiO_2 phase had minimal impact, regardless of their hydrophilic or hydrophobic properties. We compared the effects of NiTi surfaces with anatase and rutile crystalline phases on vascular cell behavior. To achieve this, we heat-treated NiTi surfaces using a radiant furnace to control the crystalline structure and subsequently cultured vascular cells on these modified NiTi surfaces (Supporting Information S6).Our results indicated that the rutile crystalline structure, predominant in the group (530 °C, 40 min), could reduce the attachment ability of SMCs. Conversely, the attachment ability of the ECs showed a similar or negligible decrease. Numerous studies have demonstrated that cell behavior and fate can be influenced by the diverse properties of the surfaces they contact, and even with identical mechanobiological characteristics, cells can exhibit varied behaviors depending on their tissue of origin [16]. Previous research has shown that ECs and SMCs respond differently to vascular injury; ECs typically shift to a mesenchymal phenotype uniformly, while SMCs exhibit varied responses, with some becoming proinflammatory and others adapting to stress [47]. This differential response underscores the importance of tailored surface modifications to optimize cell-specific

interactions and improve vascular healing outcomes. In this study, laser texturing was used to control the physical and chemical properties of NiTi surfaces, aiming to maintain EC function while inhibiting SMC hyperplasia, migration, and dedifferentiation. These results highlight the ability to control cellular behavior and functionality through the metal surface structure, size, and crystalline properties, emphasizing the need for additional comprehensive research to optimize vascular cell interactions with stent surfaces. Future studies will analyze the specific proteins and genes influenced by the physical and chemical characteristics of laser-textured NiTi to determine the distinct signals affecting the two cell types' behaviors.

3.4. Monocyte adhesion to EC layer cultured on laser-textured NiTi

We conducted a monocyte adhesion assay based on the surface properties of the laser-textured NiTi. ECs, comprising blood vessels, resist atherosclerosis and inflammation based on their structural characteristics [48,49]. We exposed ECs to TNF-α, a pro-inflammatory cytokine, to mimic the inflammatory environment associated with the early stages of atherosclerosis [49,50]. As a negative control, minimal monocyte attachment was observed when monocytes were co-cultured on the EC layer without any treatment (normal or healthy state), and there was no significant difference between groups (Supporting information S14). Additionally, ZO-1, a tight junction-associated cytoplasmic plaque protein and a reliable marker for ECs, exhibited consistently strong expression across all groups. This finding suggests that the probability of additional monocyte attachment is low in the healthy state of ECs. In contrast, EC monolayers exposed to TNF-α exhibited a significant reduction or impairment of the ZO-1 protein (Supporting information S15). When monocytes were co-cultured on the TNF-α treated EC layer, we observed a dramatic increase in monocyte adhesion. Interestingly, in the micro-W and pMW groups, minimal monocyte adhesion to the TNF-α treated EC layer was demonstrated. For instance, the number of monocytes captured to the EC monolayer grown on the control was 173.11 ± 22.63 cells/mm^2, compared to 91.45 ± 12.05 cells/mm^2 and 81.65 ± 17.71 cells/mm^2 for micro-W and pMW, respectively. These results suggest that micro-W structures on NiTi can lead to EC monolayer growth that disrupts monocyte adhesion compared with EC monolayers grown on control and nano-W structures.

We further investigated the potential mechanism by which monocyte adhesion was reduced on laser-textured NiTi by measuring the expression of several genes involved in EC maturation upon TNF-α induced inflammation, as depicted in Fig. 6d. The expression of E-selectin decreased in EC monolayers on the NiTi surface featuring micro-W patterns (0.39 ± 0.03 and 0.40 ± 0.04 for micro-W and pMW, respectively; normalized value to the control). In contrast, the nano-W and pNW groups did not differ significantly from the control group. Chemokine ligand (CCL)-2 and vascular cell adhesion molecule (VCAM)-1

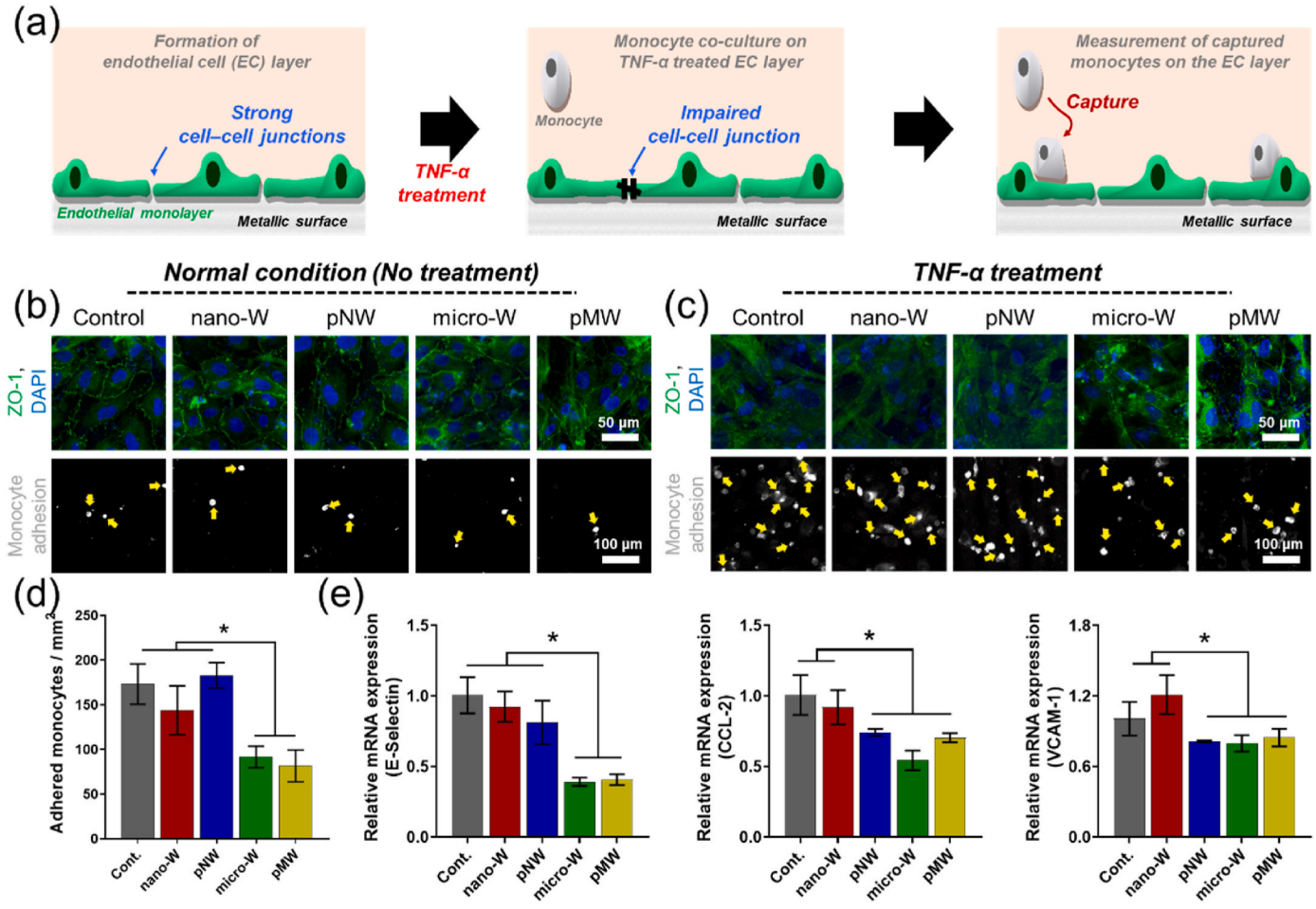

Fig. 6. (a) Schematic representation of the monocyte adhesion assay on laser-textured NiTi. Following a 24-h culture of an endothelial cell (EC) monolayer on laser-textured NiTi, treatment with tumor necrosis factor-a (TNF-α) for 12 h was performed. Vybrants DiO-labeled THP-1 monocytes were then seeded to the TNF-α-treated EC monolayer, and the measurement involved quantifying the captured monocytes on the EC layer. Representative images of the cellular distribution of ZO-1 in (b) normal EC and (c) TNF- α treated EC on laser-textured NiTi. Monocytes adhered to the (b) normal EC and (c) TNF- α treated EC on laser-textured NiTi. (DiO-labeled monocytes are indicated in white color). (d) Quantification of monocyte adhesion on the TNF-α-treated EC monolayer. (e) Relative expression of genes potentially associated with monocyte adhesion from the EC layer cultured on laser-textured NiTi following TNF-α treatment. * indicates a significant difference ($p < 0.05$, $n = 5$).

expression also decreased in the endothelial monolayers in the pNW, micro-W, and pMW groups. For example, the expression of CCL-2 exhibited 0.91 ± 0.12, 0.74 ± 0.02, 0.54 ± 0.07, and 0.71 ± 0.03 for nano-W, pNW, micro-W, and pMW, respectively. The result shows that CCL-2 and VCAM-1 gene expression decreased in the pNW group, similar to the NiTi surface featuring micro-W. Preventing monocyte adhesion in the vascular system typically requires the downregulation of inflammation-related genes such as E-selectin, VCAM1, and CCL2, which play crucial roles in mediating the adhesion and recruitment of monocytes to endothelial cells, especially under inflammatory condition [51,52]. Several reports have explained that EC monolayers with anisotropic patterns exhibit decreased inflammation responses [50,53,54]. Consistent with previous reports, laser-textured NiTi featuring micro-W reduced the expression of inflammation-related adhesion molecules. Efforts have been made to prevent atherosclerosis and inflammation during stent placement. These efforts primarily involve innovations in materials, coating technologies, medical device design, and drug delivery systems [55–58]. Our findings suggest that by controlling the physical characteristics of material surfaces through laser texturing rather than involving complex systems, there is the potential to reduce inflammation that may occur following clinical stent insertion in the future. This approach offers a simpler alternative for more complex systems, emphasizing the potential for surface texturing in biomedical applications.

3.5. Evaluation of angiogenesis capability through ex vivo model

Promoting angiogenesis during stent deployment is crucial for the rapid repair and regeneration of the endothelial layer, which is often damaged during the stent placement process. This process helps to prevent restenosis, modulate inflammation, and ensure long-term vascular health by maintaining proper blood supply and vessel functionality [6,59]. We conducted an *ex vivo* fetal mouse metatarsal angiogenesis assay to evaluate angiogenesis. *Ex vivo* approaches provide a more physiologically appropriate environment for studying biological processes to bridge the gap between *in vitro* and *in vivo* assessments [60,61]. For this purpose, a fetal mouse metatarsal assay was used on laser-textured NiTi (Fig. 7a and b). This well-established *ex vivo* model enables the observation and quantification of sprouting blood vessels in a microenvironment that closely resembles the *in vivo* formation of natural blood vessels [62,63]. The growth of vessels from isolated embryonic metatarsals within this assay captures critical aspects of natural blood vessel formation, including EC lumen formation, tip cell development, and the recruitment of adjacent support cells [64]. We suggest that the angiogenic impact can be accurately assessed by considering the properties of the metal surface and the close interaction between the vessel and the metallic surface. As shown in Fig. 7b, we confirmed increased angiogenesis in the laser-textured NiTi group (wrinkled topographies) compared to the control group. Consistent with the results obtained using ECs, we observed increased angiogenesis in the micro-W topography groups (micro-W and pMW) compared to the nano-W topography groups (nano-W and pNW). Additionally, in the pNW and

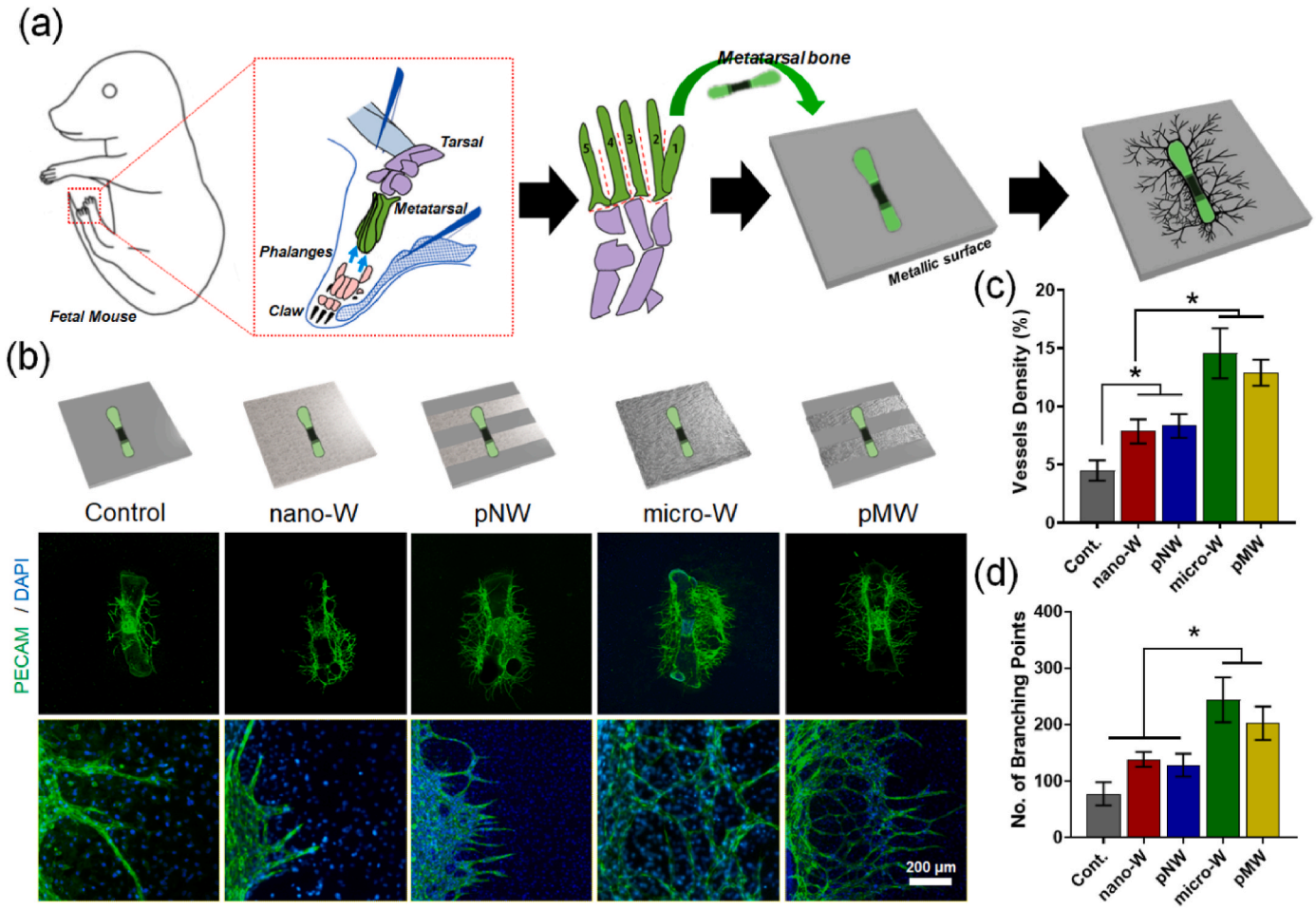

Fig. 7. (a) Schematic illustration of the fetal mouse metatarsal assay on laser-textured NiTi. (b) Representative fluorescent images of PECAM-positive vessel outgrowth from metatarsal growth on different laser-textured NiTi surfaces. Quantitative analysis of (c) vessel density and (d) the number of branching points on laser-textured NiTi. * indicates a significant difference ($p < 0.05$, $n = 4$).

pMW groups, which exhibited directional structural properties, angiogenesis was aligned with the directional pattern of the laser-textured wrinkles, indicating that it may represent a guided formation process. During the evaluation of angiogenesis, the analysis of vessel density and branching points is a key component for quantifying blood supply and assessing the complexity of the vascular network within tissues [65–67]. Higher vessel density and increased branching points are well-documented to improve tissue perfusion and oxygen delivery, which are crucial for tissue survival, adaptability, responsiveness to metabolic demands, and injury recovery, providing valuable perspectives for understanding angiogenesis's structural and functional aspects [64,65,68]. Through image-based quantitative analysis, we demonstrated statistically significant increases in vessel density and number of branching points in the micro-W and pMW groups compared to those in the other groups (Fig. 7c and d). These data indicate that laser texturing on metal surfaces has the potential to stimulate enhanced angiogenesis through specific topographical features that appear to promote angiogenesis. Interestingly, PECAM-positive vessel outgrowth from metatarsal formed in the nano-W groups (nano-W and pNW) appeared densely packed, whereas micro-W and pMW exhibited more scattered patterns (Supporting Information S16). Although we focused on analyzing angiogenesis restricted to endothelialization through imaging results in this study, our future research will broaden the scope to focus on various cell types such as ECs, nerve cells, perivascular mural cells, and macrophages [64] generated from metatarsal bone cultured on the surfaces of laser-textured NiTi.

4. Conclusion

While laser texturing of NiTi surfaces is an established technique, this study provides novel insights into how specific micro- and nano-scale patterns can precisely modulate cellular behaviors relevant to vascular responses. Our comprehensive analysis from cellular assays to *ex vivo* angiogenesis assays demonstrated distinct responses from ECs and SMCs. We showed that laser-textured NiTi surfaces with microscale wrinkle structures (micro-W and pMW) effectively prevent various cellular phenomena contributing to restenosis, such as SMC dedifferentiation, migration, and monocyte adhesion to TNF-α treated EC layers. Specifically, surfaces with microscale wrinkles showed increased endothelialization markers, particularly endothelial phenotype genes such as Tie-2 and vWF. Further investigations using an *ex vivo* fetal mouse metatarsal assay revealed that laser-textured surfaces significantly enhance angiogenesis, with micro-W patterns increasing vessel density and branching, essential for tissue survival and adaptability. These findings suggest that the angiogenic potential of microscale wrinkle surfaces on NiTi supports tissue survival and responsiveness through improved vascularization. This research bridges the gap between *in vitro* and *in vivo* studies, offering promising preliminary insights into how specific topographical features of stent surfaces influence cellular behavior and angiogenesis. While this study was conducted on NiTi alloy plates rather than medical stents, the findings offer promising and preliminary insights into stent technology advancements. Our future research will apply these insights to the surface design of stents and other implantable materials, aiming for improved biocompatibility, reduced inflammation, and enhanced vascular regeneration.

Ethics approval and consent to participate

The fetal metatarsal angiogenesis assays were performed in accordance with the relevant guidelines and regulations of the Institutional Animal Care and Use Committee (IACUC) and the Institutional Biosafety Committee (IBC) at KIST (Approval number KIST-IACUC-2023-043-1).

CRediT authorship contribution statement

Indong Jun: Writing – review & editing, Writing – original draft, Investigation, Formal analysis, Data curation, Conceptualization. **Haneul Choi:** Investigation, Data curation, Conceptualization. **Hyeok Kim:** Validation, Formal analysis, Data curation. **Byoung Chan Choi:** Investigation, Data curation. **Hye Jung Chang:** Methodology, Investigation. **Youngjun Kim:** Supervision, Methodology, Conceptualization. **Sung Woo Cho:** Methodology, Investigation. **James R. Edwards:** Supervision, Conceptualization. **Suk-Won Hwang:** Supervision, Methodology, Investigation, Conceptualization. **Yu-Chan Kim:** Resources, Funding acquisition, Conceptualization. **Hyung-Seop Han:** Writing – original draft, Supervision, Project administration, Investigation. **Hojeong Jeon:** Writing – original draft, Supervision, Investigation, Formal analysis, Conceptualization.

Declaration of competing interest

Hyung-Seop Han is an editorial board member for Bioactive Materials and was not involved in the editorial review or the decision to publish this article. All authors declare that there are no competing interests.

Acknowledgments

This work was supported by a KIST project [2E32351, 2E33122, 2V09840-23-P023], and the KU-KIST Graduate School of Converging Science and Technology Program. This research was also supported by a National Research Foundation of Korea (NRF) grant funded by the Korean government (MSIT) [grant number RS-2023-00302145]. This research was supported by the Bio-cluster Industry Capacity Enhancement Project of Jeonbuk Technopark (JBTP). Additionally, H.J. and Y.C. K. were supported by the Korea Medical Device Development Fund grant funded by the Korean government (the Ministry of Science and ICT, the Ministry of Trade, Industry and Energy, the Ministry of Health & Welfare, and the Ministry of Food and Drug Safety) (NTIS Number: 9991007189). Furthermore, H.J. Chang and H. Choi were supported by the Ministry of Trade, Industry, and Energy (MOTIE) of Korea through project No. P0022331, supervised by the Korea Institute for Advancement of Technology (KIAT).

Appendix A. Supplementary data

Supplementary data to this article can be found online at https://doi.org/10.1016/j.bioactmat.2024.09.019.

References

[1] M. Gaudino, F. Andreotti, T. Kimura, Current concepts in coronary artery revascularisation, Lancet 401 (10388) (2023) 1611–1628.
[2] R. Piccolo, K.H. Bonaa, O. Efthimiou, O. Varenne, A. Baldo, P. Urban, C. Kaiser, W. Remkes, L. Raber, A. de Belder, A.W.J. van 't Hof, G. Stankovic, P.A. Lemos, T. Wilsgaard, J. Reifart, A.E. Rodriguez, E.E. Ribeiro, P. Serruys, A. Abizaid, M. Sabate, R.A. Byrne, J.M. de la Torre Hernandez, W. Wijns, P. Juni, S. Windecker, M. Valgimigli, C. Coronary Stent Trialists, Drug-eluting or bare-metal stents for percutaneous coronary intervention: a systematic review and individual patient data meta-analysis of randomised clinical trials, Lancet 393 (10190) (2019) 2503–2510.
[3] J. Dong, M. Pacella, Y. Liu, L. Zhao, Surface engineering and the application of laser-based processes to stents - a review of the latest development, Bioact. Mater. 10 (2022) 159–184.
[4] J. Zong, Q. He, Y. Liu, M. Qiu, J. Wu, B. Hu, Advances in the development of biodegradable coronary stents: a translational perspective, Mater Today Bio 16 (2022) 100368.
[5] A. Autar, A. Taha, R. van Duin, I. Krabbendam-Peters, D.J. Duncker, F. Zijlstra, H. M.M. van Beusekom, Endovascular procedures cause transient endothelial injury but do not disrupt mature neointima in Drug Eluting Stents, Sci. Rep. 10 (1) (2020) 2173.
[6] A. Cornelissen, F.J. Vogt, The effects of stenting on coronary endothelium from a molecular biological view: time for improvement? J. Cell Mol. Med. 23 (1) (2019) 39–46.
[7] R. Chakraborty, P. Chatterjee, J.M. Dave, A.C. Ostriker, D.M. Greif, E.M. Rzucidlo, K.A. Martin, Targeting smooth muscle cell phenotypic switching in vascular disease, JVS Vasc Sci 2 (2021) 79–94.

[8] Y. Zhuang, C. Zhang, M. Cheng, J. Huang, Q. Liu, G. Yuan, K. Lin, H. Yu, Challenges and strategies for in situ endothelialization and long-term lumen patency of vascular grafts, Bioact. Mater. 6 (6) (2021) 1791–1809.
[9] R.A. Byrne, G.W. Stone, J. Ormiston, A. Kastrati, Coronary balloon angioplasty, stents, and scaffolds, Lancet 390 (10096) (2017) 781–792.
[10] A.S. Khalil, R. Jaenisch, D.J. Mooney, Engineered tissues and strategies to overcome challenges in drug development, Adv. Drug Deliv. Rev. 158 (2020) 116–139.
[11] E.E. Marr, B.C. Isenberg, J.Y. Wong, Effects of polydimethylsiloxane membrane surface treatments on human uterine smooth muscle cell strain response, Bioact. Mater. 32 (2024) 415–426.
[12] N.O. Monteiro, J.F. Fangueiro, R.L. Reis, N.M. Neves, Replication of natural surface topographies to generate advanced cell culture substrates, Bioact. Mater. 28 (2023) 337–347.
[13] I. Jun, Y.W. Chung, J. Park, H.S. Han, J. Park, S. Kim, H. Lee, S.H. Kim, J.H. Han, H. Kim, H.K. Seok, Y.C. Kim, H. Jeon, Ultrathin metal films with defined topographical structures as in vitro cell culture platforms for unveiling vascular cell behaviors, Adv. Healthcare Mater. 5 (18) (2016) 2396–2405.
[14] C. Han, X. Luo, D. Zou, J. Li, K. Zhang, P. Yang, N. Huang, Nature-inspired extracellular matrix coating produced by micro-patterned smooth muscle and endothelial cells endows cardiovascular materials with better biocompatibility, Biomater. Sci. 7 (7) (2019) 2686–2701.
[15] K. Zhou, Y. Li, L. Zhang, L. Jin, F. Yuan, J. Tan, G. Yuan, J. Pei, Nano-micrometer surface roughness gradients reveal topographical influences on differentiating responses of vascular cells on biodegradable magnesium, Bioact. Mater. 6 (1) (2021) 262–272.
[16] B. Yi, Q. Xu, W. Liu, An overview of substrate stiffness guided cellular response and its applications in tissue regeneration, Bioact. Mater. 15 (2022) 82–102.
[17] A. Papadopoulos, E. Skoulas, A. Mimidis, G. Perrakis, G. Kenanakis, G.D. Tsibidis, E. Stratakis, Biomimetic omnidirectional antireflective glass via direct ultrafast laser nanostructuring, Adv. Mater. 31 (32) (2019) e1901123.
[18] S.H. Um, J. Lee, I.S. Song, M.R. Ok, Y.C. Kim, H.S. Han, S.H. Rhee, H. Jeon, Regulation of cell locomotion by nanosecond-laser-induced hydroxyapatite patterning, Bioact. Mater. 6 (10) (2021) 3608–3619.
[19] I. Jun, N. Li, J. Shin, J. Park, Y.J. Kim, H. Jeon, H. Choi, J.G. Cho, B. Chan Choi, H. S. Han, J.J. Song, Synergistic stimulation of surface topography and biphasic electric current promotes muscle regeneration, Bioact. Mater. 11 (2022) 118–129.
[20] A. Cholkar, R. McCann, G. Perumal, S. Chatterjee, M. Swayne, D. Kinahan, D. Brabazon, Advances in laser-based surface texturing for developing antifouling surfaces: a comprehensive review, Applied Surface Science Advances 18 (2023) 100513.
[21] C.H. Fu, J.F. Liu, A. Guo, Statistical characteristics of surface integrity by fiber laser cutting of Nitinol vascular stents, Appl. Surf. Sci. 353 (2015) 291–299.
[22] C.A. Biffi, J. Fiocchi, A. Tuissi, Relevant aspects of laser cutting of NiTi shape memory alloys, J. Mater. Res. Technol. 19 (2022) 472–506.
[23] N. Maharjan, W. Zhou, Y. Zhou, Y. Guan, N. Wu, Comparative study of laser surface hardening of 50CrMo4 steel using continuous-wave laser and pulsed lasers with ms, ns, ps and fs pulse duration, Surf. Coating. Technol. 366 (2019) 311–320.
[24] Y. Lu, Y. Guan, Y. Li, L. Yang, M. Wang, Y. Wang, Nanosecond laser fabrication of superhydrophobic surface on 316L stainless steel and corrosion protection application, Colloids Surf. A Physicochem. Eng. Asp. 604 (2020) 125259.
[25] A. He, W. Liu, W. Xue, H. Yang, Y. Cao, Nanosecond laser ablated copper superhydrophobic surface with tunable ultrahigh adhesion and its renewability with low temperature annealing, Appl. Surf. Sci. 434 (2018) 120–125.
[26] K. Yu, H. Shi, P. Zhang, Z. Yu, H. Yan, Q. Lu, Micro/nanoengineering of functionalized metal surfaces based on short/ultra-short-pulsed lasers: a review, J. Mater. Sci. 59 (5) (2024) 1819–1866.
[27] Z. Liu, T. Niu, Y. Lei, Y. Luo, Metal surface wettability modification by nanosecond laser surface texturing: a review, Biosurface and Biotribology 8 (2) (2022) 95–120.
[28] J. Zhou, H. Shen, Y. Pan, X. Ding, Experimental study on laser microstructures using long pulse, Opt Laser. Eng. 78 (2016) 113–120.
[29] C.M. Dumont, J. Park, L.D. Shea, Controlled release strategies for modulating immune responses to promote tissue regeneration, J. Contr. Release 219 (2015) 155–166.
[30] B.N. Kharbikar, P. Mohindra, T.A. Desai, Biomaterials to enhance stem cell transplantation, Cell Stem Cell 29 (5) (2022) 692–721.
[31] P. Jiang, Y. Zhang, R. Hu, X. Wang, Y. Lai, G. Rui, C. Lin, Hydroxyapatite-modified micro/nanostructured titania surfaces with different crystalline phases for osteoblast regulation, Bioact. Mater. 6 (4) (2021) 1118–1129.
[32] K. Bourikas, C. Kordulis, A. Lycourghiotis, Titanium dioxide (anatase and rutile): surface chemistry, liquid-solid interface chemistry, and scientific synthesis of supported catalysts, Chem. Rev. 114 (19) (2014) 9754–9823.
[33] B. Clarke, W. Carroll, Y. Rochev, M. Hynes, D. Bradley, D. Plumley, Influence of Nitinol wire surface treatment on oxide thickness and composition and its subsequent effect on corrosion resistance and nickel ion release, J. Biomed. Mater. Res. 79 (1) (2006) 61–70.
[34] W.S. Chan, K. Gulati, O.A. Peters, Advancing Nitinol: from heat treatment to surface functionalization for nickel-titanium (NiTi) instruments in endodontics, Bioact. Mater. 22 (2023) 91–111.
[35] K. Niitsu, Y. Kimura, X. Xu, R. Kainuma, Composition dependences of entropy change and transformation temperatures in Ni-rich Ti–Ni system, Shape Memory and Superelasticity 1 (2) (2015) 124–131.
[36] H. Choi, M.Y. Na, I. Jun, H. Jeon, Y.-C. Kim, J.-W. Park, H.J. Chang, Repetitive nanosecond laser-induced oxidation and phase transformation in NiTi alloy, Met. Mater. Int. 30 (5) (2024) 1200–1208.
[37] D.A.H. Hanaor, C.C. Sorrell, Review of the anatase to rutile phase transformation, J. Mater. Sci. 46 (4) (2011) 855–874.
[38] M. Ermis, E. Antmen, V. Hasirci, Micro and Nanofabrication methods to control cell-substrate interactions and cell behavior: a review from the tissue engineering perspective, Bioact. Mater. 3 (3) (2018) 355–369.
[39] H. Yao, Y. He, J. Ma, L. Jiang, J. Li, J. Wang, N. Huang, Recent advances in cardiovascular stent for treatment of in-stent restenosis: mechanisms and strategies, Chin. J. Chem. Eng. 37 (2021) 12–29.
[40] G. Yang, B. Mahadik, J.Y. Choi, J.P. Fisher, Vascularization in tissue engineering: fundamentals and state-of-art, Prog. Biomed. Eng. 2 (1) (2020).
[41] M. Nakhaei-Nejad, M. Farhan, A. Mojiri, H. Jabbari, A.G. Murray, N. Jahroudi, Regulation of von Willebrand Factor Gene in Endothelial Cells That Are Programmed to Pluripotency and Differentiated Back to Endothelial Cells, Stem Cell. 37 (4) (2019) 542–554.
[42] G. Cao, X. Xuan, J. Hu, R. Zhang, H. Jin, H. Dong, How vascular smooth muscle cell phenotype switching contributes to vascular disease, Cell Commun. Signal. 20 (1) (2022) 180.
[43] M. Liu, D. Gomez, Smooth muscle cell phenotypic diversity, Arterioscler. Thromb. Vasc. Biol. 39 (9) (2019) 1715–1723.
[44] J.M. Miano, E.A. Fisher, M.W. Majesky, Fate and state of vascular smooth muscle cells in atherosclerosis, Circulation 143 (21) (2021) 2110–2116.
[45] S. Fleischer, D.N. Tavakol, G. Vunjak-Novakovic, From arteries to capillaries: approaches to engineering human vasculature, Adv. Funct. Mater. 30 (37) (2020).
[46] Y. Suzuki, G. Ichihara, S. Kawada, K.i. Miyazawa, T. Furutani, A. Hayashida, E. Watanabe, C. Zong, L. Tran, A. Ikegami, S. Ichihara, Effects of physiochemical characteristic of nano-sized TiO2 on the adhesion of monocytes to endothelial cells, NanoImpact 20 (2020) 100257.
[47] X. Ding, Q. An, W. Zhao, Y. Song, X. Tang, J. Wang, C.C. Chang, G. Zhao, T. Hsiai, G. Fan, Y. Fan, S. Li, Distinct patterns of responses in endothelial cells and smooth muscle cells following vascular injury, JCI Insight 7 (20) (2022).
[48] B.E. Sansbury, M. Spite, Resolution of acute inflammation and the role of resolvins in immunity, thrombosis, and vascular biology, Circ. Res. 119 (1) (2016) 113–130.
[49] S. Xu, I. Ilyas, P.J. Little, H. Li, D. Kamato, X. Zheng, S. Luo, Z. Li, P. Liu, J. Han, I. C. Harding, E.E. Ebong, S.J. Cameron, A.G. Stewart, J. Weng, Endothelial dysfunction in atherosclerotic cardiovascular diseases and beyond: from mechanism to pharmacotherapies, Pharmacol. Rev. 73 (3) (2021) 924–967.
[50] Y.M. Shin, H.J. Shin, Y. Heo, I. Jun, Y.-W. Chung, K. Kim, Y.M. Lim, H. Jeon, H. Shin, Engineering an aligned endothelial monolayer on a topologically modified nanofibrous platform with a micropatterned structure produced by femtosecond laser ablation, J. Mater. Chem. B 5 (2) (2017) 318–328.
[51] A. Gatsiou, S. Tual-Chalot, M. Napoli, A. Ortega-Gomez, T. Regen, R. Badolia, V. Cesarini, C. Garcia-Gonzalez, R. Chevre, G. Ciliberti, C. Silvestre-Roig, M. Martini, J. Hoffmann, R. Hamouche, J.R. Visker, N. Diakos, A. Wietelmann, D. A. Silvestris, G. Georgiopoulos, A. Moshfegh, A. Schneider, W. Chen, S. Guenther, J. Backs, S. Kwak, C.H. Selzman, K. Stamatelopoulos, S. Rose-John, C. Trautwein, I. Spyridopoulos, T. Braun, A. Waisman, A. Gallo, S.G. Drakos, S. Dimmeler, M. Sperandio, O. Soehnlein, K. Stellos, The RNA editor ADAR2 promotes immune cell trafficking by enhancing endothelial responses to interleukin-6 during sterile inflammation, Immunity 56 (5) (2023) 979–997 e911.
[52] G. Kaur, D. Sharma, S. Bisen, C.S. Mukhopadhyay, K. Gurdziel, N.K. Singh, Vascular cell-adhesion molecule 1 (VCAM-1) regulates JunB-mediated IL-8/CXCL1 expression and pathological neovascularization, Commun. Biol. 6 (1) (2023) 516.
[53] G. Stefopoulos, C. Giampietro, V. Falk, D. Poulikakos, A. Ferrari, Facile endothelium protection from TNF-alpha inflammatory insult with surface topography, Biomaterials 138 (2017) 131–141.
[54] M.E. Fallon, M.T. Hinds, Single cell morphological metrics and cytoskeletal alignment regulate VCAM-1 protein expression, Biochem. Biophys. Res. Commun. 555 (2021) 160–167.
[55] S. Chen, Z. Yao, Y. Guan, H. Yang, M.B. Shahzad, Y. Wu, B. Zhang, L. Shen, K. Yang, High nitrogen stainless steel drug-eluting stent - assessment of pharmacokinetics and preclinical safety in vivo, Bioact. Mater. 5 (4) (2020) 779–786.
[56] S. Ravanbakhsh, C. Paternoster, G. Barucca, P. Mengucci, S. Gambaro, T. Lescot, P. Chevallier, M.A. Fortin, D. Mantovani, Improving the radiopacity of Fe-Mn biodegradable metals by magnetron-sputtered W-Fe-Mn-C coatings: application for thinner stents, Bioact. Mater. 12 (2022) 64–70.
[57] J. Wang, H.L. Qian, S.Y. Chen, W.P. Huang, D.N. Huang, H.Y. Hao, K.F. Ren, Y. B. Wang, G.S. Fu, J. Ji, miR-22 eluting cardiovascular stent based on a self-healable spongy coating inhibits in-stent restenosis, Bioact. Mater. 6 (12) (2021) 4686–4696.
[58] R. Wang, J. Lu, J. Yin, H. Chen, H. Liu, F. Xu, T. Zang, R. Xu, C. Li, Y. Wu, Q. Wu, X. Fei, M. Zhu, L. Shen, J. Ge, A TEMPOL and rapamycin loaded nanofiber-covered stent favors endothelialization and mitigates neointimal hyperplasia and local inflammation, Bioact. Mater. 19 (2023) 666–677.
[59] R.C. Goncalves, A. Banfi, M.B. Oliveira, J.F. Mano, Strategies for re-vascularization and promotion of angiogenesis in trauma and disease, Biomaterials 269 (2021) 120628.
[60] D. Shi, G. Mi, M. Wang, T.J. Webster, In vitro and ex vivo systems at the forefront of infection modeling and drug discovery, Biomaterials 198 (2019) 228–249.
[61] Y. Xu, N. Shrestha, V. Preat, A. Beloqui, An overview of in vitro, ex vivo and in vivo models for studying the transport of drugs across intestinal barriers, Adv. Drug Deliv. Rev. 175 (2021) 113795.
[62] F.C. Cackowski, J.L. Anderson, K.D. Patrene, R.J. Choksi, S.D. Shapiro, J.J. Windle, H.C. Blair, G.D. Roodman, Osteoclasts are important for bone angiogenesis, Blood 115 (1) (2010) 140–149.

[63] H.S. Han, I. Jun, H.K. Seok, K.S. Lee, K. Lee, F. Witte, D. Mantovani, Y.C. Kim, S. Glyn-Jones, J.R. Edwards, Biodegradable magnesium alloys promote angio-osteogenesis to enhance bone repair, Adv. Sci. 7 (15) (2020) 2000800.
[64] W. Song, C.W. Fhu, K.H. Ang, C.H. Liu, N.A.B. Johari, D. Lio, S. Abraham, W. Hong, S.E. Moss, J. Greenwood, X. Wang, The fetal mouse metatarsal bone explant as a model of angiogenesis, Nat. Protoc. 10 (10) (2015) 1459–1473.
[65] F. Mirzapour-Shafiyi, Y. Kametani, T. Hikita, Y. Hasegawa, M. Nakayama, Numerical evaluation reveals the effect of branching morphology on vessel transport properties during angiogenesis, PLoS Comput. Biol. 17 (6) (2021) e1008398.
[66] J. Ehling, B. Theek, F. Gremse, S. Baetke, D. Mockel, J. Maynard, S.A. Ricketts, H. Grull, M. Neeman, R. Knuechel, W. Lederle, F. Kiessling, T. Lammers, Micro-CT imaging of tumor angiogenesis: quantitative measures describing micromorphology and vascularization, Am. J. Pathol. 184 (2) (2014) 431–441.
[67] A.V. Benest, D.O. Bates, Measurement of angiogenic phenotype by use of two-dimensional mesenteric angiogenesis assay, Methods Mol. Biol. 467 (2009) 251–270.
[68] A.N. Ivanov, Y.R. Chabbarov, Mechanisms of physiological angiogenesis, J. Evol. Biochem. Physiol. 59 (3) (2023) 914–929.